Electrochemical Deposition of Bis(*N,N′*-diphenylaminoaryl) Substituted Ferrocenes, and Their Application as a Hole-Injection Layer on Polymeric Light-Emitting Diodes

Chao Cheng Chiang,[†] Hong-Chun Chen,[†] Chin-sheng Lee,[†] Man-kit Leung,*[,†,‡] Kun-Rung Lin,[‡] and Kuo-Huang Hsieh[‡]

Department of Chemistry and Institute of Polymer Science and Engineering, National Taiwan University, 1 Roosevelt Road, Section 4, Taipei 106, Taiwan, ROC

Received August 7, 2007. Revised Manuscript Received October 30, 2007

The synthesis, spectro-electrochemical study, and electrochemical polymerization of bis(diphenylamino) substituted ferrocenes (Fcs), including the family of the 1,3,4-oxadiazole (OXD) bridged 1,1′-[*p*-$(Ph_2N)(C_6H_4)_n$OXD]$_2$Fc and the vinylene bridged ferrocene 1,1′-[*p*-$(Ph_2N)(C_6H_4)$-(*E*)-CH=CH]$_2$Fc, have been carried out. The ferrocene compounds underwent three stepwise one-electron oxidations to form the (3+) radical cations that further electrochemically polymerized on a Pt or an indium tin oxide (ITO) electrode surface. The polymeric layers showed extremely good hole-injection properties. The polymeric light emitting devices (PLEDs) of ITO/ED-1,1′-[$Ph_2N(C_6H_4)_3$OXD]$_2$Fc/PVK:Ir(PPy)$_3$:PBD/Mg-Ag showed a turn-on voltage (at 100 cd/m^2) of 11 V, with a maximum brightness of 27 700 cd/m^2. The turn-on voltage was 1.5 V lower than that of the poly(3,4-ethylenedioxythiophene)poly(styrenesulfonate) based PLED and 2 V lower than the corresponding electrochemically deposited poly(4-(*N,N*-diphenylamino)styrene) based PLED.

Introduction

Considerable efforts have been paid to the development of new electroactive polymers.[1] These materials can be used in organic electronic devices,[2] sensors,[3] polymer batteries,[4] electrochromic devices,[5] or polymeric light emitting diodes.[6] Conjugated polymers containing organometallic complexes or coordination complexes in the backbone or on the side chains are of particular interest because many metal containing cores could be reversibly switched between the redox states.[7] By varying the redox states of the metal core, the conductivity, optical properties, and electronic behavior of the conjugated polymers could be modulated. Ferrocene is a well-known electrochemically active compound which shows good electron-transfer properties.[8] Incorporation of ferrocene units into polymers has therefore attracted a lot of attention.[9] In addition, as a result of the substituent effect on the oxidation potential of the ferrocene, the highest occupied and the lowest unoccupied molecular orbital levels of the ferrocene could therefore be tuned by varying the substituent attached to the cyclopentadienyl rings.[10] This provides a wide window for tuning and matching the energy levels with different types of electronic materials in multilayer organic optoelectronic devices.

Electrochemical coupling is an established technique for the preparation of polymeric film on the conducting electrodes. Many heterocyclic moieties including thiophene, pyrrole, arylamine, and carbazole are active toward the coupling conditions and have been used as the handle for electrochemical polymerization.[11] For example, Zhu and Wolf have reported the study of oligothienylferrocene **1**.[12] Constable and Hagfeldt et al. have prepared a rodlike

* Corresponding author. E-mail: mkleung@ntu.edu.tw.
† Department of Chemistry.
‡ Institute of Polymer Science and Engineering.

(1) Vinogradov, A.; Su, J.; Jenkins, C.; Bar-Cohen, Y. *Mater. Res. Soc. Symp. Proc.* **2006**, *889*, 51.
(2) (a) Chidsey, C. E. D.; Murray, R. W. *Science* **1986**, *231*, 25. (b) Garnier, F.; Hajlaoui, R.; Yassar, A.; Srivastava, P. *Science* **1994**, *265*, 1684. (c) Wrighton, M. S. *Science* **1986**, *231*, 32.
(3) (a) Thackeray, J. W.; White, H. S.; Wrighton, M. S. *J. Phys. Chem.* **1985**, *89*, 5133. (b) Fortier, G.; Brassard, E.; Belanger, D. *Biosens. Bioelectron.* **1990**, 473. (c) Bartlett, P. N.; Whithaker, R. G. *J. Electroanal. Chem.* **1987**, *224*, 27.
(4) Novak, P.; Muller, K.; Santhanam, K. S. V.; Haas, O. *Chem. Rev.* **1997**, *97*, 207.
(5) (a) Walczak, R. M.; Reynolds, J. R. *Adv. Mater.* **2006**, *18*, 1121. (b) Sonmez, G.; Sonmez, H. B.; Shen, C. K. F.; Wudl, F. *Adv. Mater.* **2004**, *16*, 1905.
(6) (a) Jungermann, S.; Riegel, N.; Müller, D.; Meerholz, K.; Nuyken, O. *Macromolecules* **2006**, *39*, 8911. (b) Deng, L.; Furuta, P. T.; Garon, S.; Li, J.; Kavulak, D.; Thompson, M. E.; Fréchet, J. M. J. *Chem. Mater.* **2006**, *18*, 386.
(7) Kaufman, F. B.; Schroeder, A. H.; Engler, E. M.; Kramer, S. R.; Chambers, J. Q. *J. Am. Chem. Soc.* **1980**, *102*, 483.
(8) (a) Kurihara, M.; Kubo, K.; Horikoshi, T.; Kurosawa, M.; Nankawa, T.; Matsuda, T.; Nishihara, H. *Macromol. Symp.* **2000**, 156. (b) Kurihara, M.; Nishihara, H. *Coord. Chem. Rev.* **2002**, *226*, 25.
(9) (a) Abd-El-Aziz, A. S.; Manners, I. *J. Inorg. Organomet. Polym.* **2005**, *15*, 157. (b) Hudson, R. D. A. *J. Organomet. Chem.* **2001**, *637–639*, 47–69. (c) Wong, W. Y.; Wong, W. K.; Raithby, P. R. *J. Chem. Soc., Dalton Trans.* **1998**, 2761.
(10) Hennig, H.; Guertler, O. *J. Organomet. Chem.* **1968**, *11*, 307.
(11) (a) Roncali, J. *J. Mater. Chem.* **1999**, *9*, 1875; *Chem. Rev.* **1992**, *92*, 71138. (b) Sabouraud, G.; Sadki, S.; Brodie, N. *Chem. Soc. Rev.* **2000**, *29*, 283. (c) Wolf, M. O.; Zhu, Y. *Adv. Mater.* **2000**, *12*, 599. (d) Natera, J.; Otero, L.; Sereno, L.; Fungo, F.; Wang, N.-S.; Tsai, Y.-M.; Hwu, T.-Y.; Wong, K.-T. *Macromolecules* **2007**, *40*, 4456. (e) Turbiez, M.; Frere, P.; Allain, M.; Gallego-Planas, N.; Roncali, J. *Macromolecules* **2005**, *38*, 6806. (f) Bueschel, M.; Ajayaghosh, A.; Eldo, J.; Daub, J. *Macromolecules* **2002**, *35*, 8405. (g) Deng, S.; Advincula, R. C. *Chem. Mater.* **2002**, *14*, 4073. (h) Hay, C.; Fischmeister, C.; Hissler, M.; Toupet, L.; Reau, R. *Angew. Chem., Int. Ed* **2000**, *39*, 1812.

10.1021/cm702217u CCC: $40.75
Published on Web 12/22/2007

Scheme 1. Oxidative Coupling of Triphenylamine

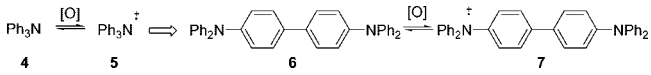

polymer containing $Ru(terpy)_2$ units by the electrochemical coupling of **2**.[13] Balch et al. adopted the approach of reductive coupling using C_{60}−Pd as the active components to prepare the ferrocene-containing thin film from **3**.[14]

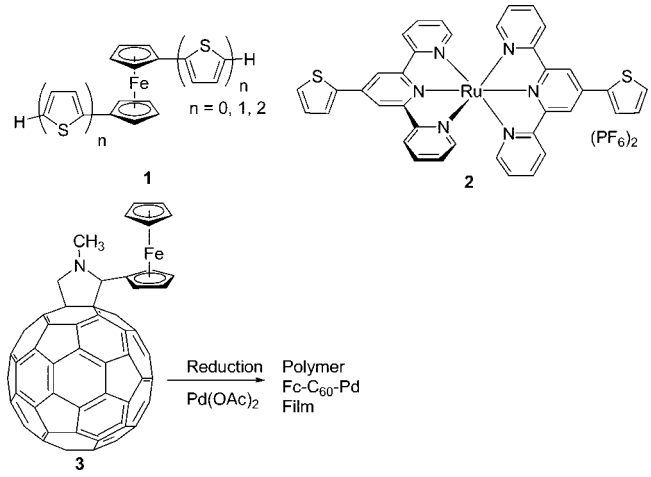

Triphenylamine (**4**) and its derivatives are known hole-transport materials that played important roles in organic light emitting devices as well as in organic electronics.[15] Recently, we have been interested in using triarylamine derivatives as handles for electropolymerization.[16] **4** is an electron-rich compound that could be oxidized to form the radical cation **5** (Scheme 1). The radical cation is reactive and dimerizes to form 4,4′-bis(*N,N*-diphenylamino)biphenyl (**6**). Although **6** could also be oxidized to form the radical cation **7**, the oxidative coupling of the radical cations is relatively sluggish because of the resonance stabilization.[17] Therefore, only oligomers would be obtained even when electropolymerization of **4** was carried out at a high concentration.[18]

Interestingly, the resonance stabilization could be blocked by inserting an electron-deficient group in between the triphenylamine units.[16b] In this situation, the chemical reactivity of the terminal triphenylamine units could therefore be resumed and the electropolymerization would occur effectively even in a diluted solution (Scheme 2).

Herein, we integrated the ferrocene and the triphenylamine moieties to form new families of electrochemically active materials. We were interested in understanding the electropolymerization behavior of the two types of ferrocene derivatives **8**−**10** and **11**.

Scheme 2. Electropolymerization of Bis-diphenylamino Substituted Compounds

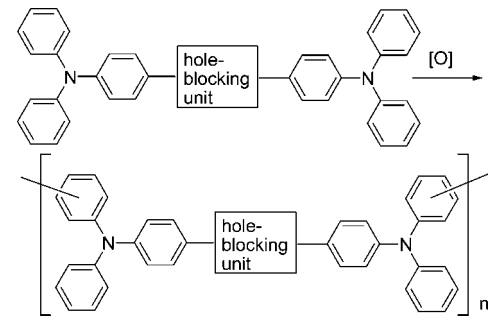

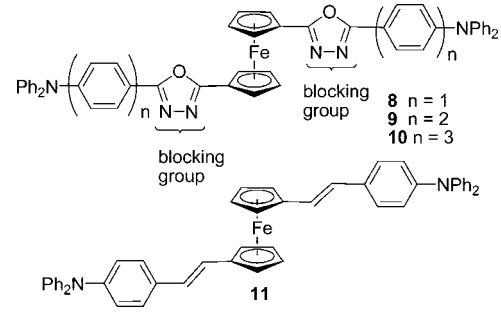

In the first type of ferrocene compounds, the ferrocene cores of **8**–**10** were separated from the electron-rich triphenylamine moieties by electron-deficient oxadiazole units. On the other hand, the ferrocene core of **11** was conjugatively linked to the triphenylamine moieties by two olefinic bridges. In addition, the possibility of using the electrochemically deposited thin films as the hole-injection layer (HIL) for the polymeric light emitting diodes was investigated.

Results and Discussion

Preparation of the Target Ferrocene Derivatives 8–11. The starting ferrocenedicarboxylate dimethyl ester **12** was prepared from the esterification of the commercially available 1,1′-ferrocenedicarboxylic acid in MeOH using concentrated sulfuric acid as the catalyst.[19] The treatment of **12** with $NH_2NH_2 \cdot H_2O$ in toluene−ethanol at the reflux temperature afforded the carbohydrazide intermediate that was further reacted with benzoyl chloride to give **13** in a high yield (Scheme 3).[20] Compound **14** was obtained smoothly from **12** under similar reaction conditions. However, we faced difficulty in the subsequent step of the dehydrative ring-closure reaction. The common cyclization−dehydration of the hydrazide precursors using $POCl_3$ as the dehydrating agent was unsuccessful, resulting in an unidentified product that was highly insoluble in organic solvents. Another approach of oxadiazole formation through intermolecular condensation of 5-(4-bromophenyl)-1*H*-tetrazole[21] with 1,1′-

(12) Zhu, Y.; Wolf, M. O. *Chem. Mater.* **1999**, *11*, 2995.
(13) Hjeim, J.; Constable, E. C.; Figgemeier, E.; Hagfeldt, A.; Handel, R.; Housecroft, C. E.; Mukhtar, E.; Schofield, E. *Chem. Commun.* **2002**, 284.
(14) Plonsk, M. E.; de Bettencourt-Dias, A; Balch, A. L.; Winkler, K. *Chem. Mater.* **2003**, *15*, 4122.
(15) (a) Shirota, Y. *J. Mater. Chem.* **2005**, *15*, 75. (b) Shirota, Y. *J. Mater. Chem.* **2000**, *10*, 1.
(16) (a) Chou, M.-Y.; Leung, M.-k.; Su, Y. O.; Chiang, C. L.; Lin, C.-C.; Liu, J.-H.; Kuo, C.-K.; Mou, C.-Y. *Chem. Mater.* **2004**, *16*, 654. (b) Leung, M.-k.; Chou, M.-Y.; Su, Y. O.; Chiang, C. L.; Chen, H.-L.; Yang, C. F.; Yang, C.-C.; Lin, C.-C; Chen, H.-T. *Org. Lett.* **2003**, *5*, 839.
(17) Seo, E. T.; Nelson, R. F.; Fritsch, J. M.; Marcoux, L. S.; Leedy, D. W.; Adams, R. N. *J. Am. Chem. Soc.* **1966**, *88*, 3498.
(18) (a) Petr, A.; Kvarnstïom, C.; Dunsch, L; Ivaska, A. *Synth. Met.* **2000**, *108*, 245. (b) Lambert, C.; Nöll, G. *Synth. Met.* **2003**, *139*, 57.
(19) (a) Anderson, J. C.; White, C.; Stenson, K. P. *Synlett* **2002**, 1511. (b) Pagel, K.; Werner, A.; Friedrichsen, W. *J. Organomet. Chem.* **1994**, *481*, 109.
(20) (a) Li, M.; Cai, P.; Duan, C.; Lu, F.; Xie, J.; Meng, Q. *Inorg. Chem.* **2004**, *43*, 5174.
(21) Schmidt, B.; Meid, D.; Kieser, D. *Tetrahedron* **2007**, *63*, 492.

Scheme 3. Synthesis of 15 and 16

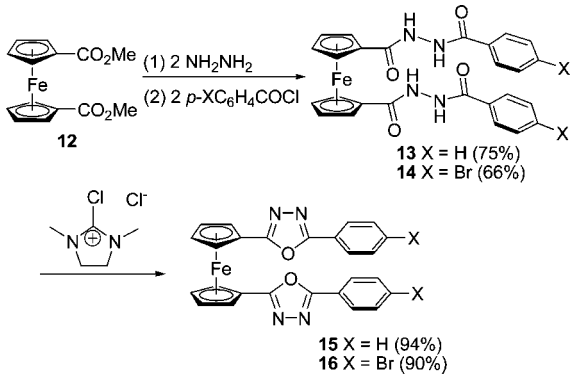

Scheme 4. Synthesis of 9, 10, and 17

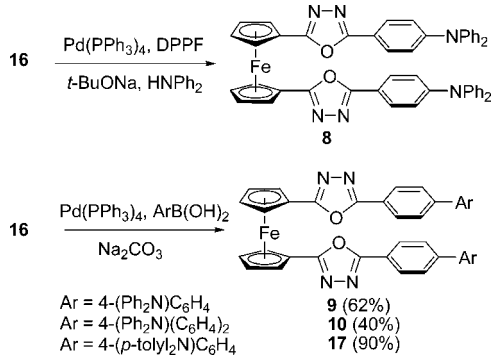

bis(chlorocarbonyl)ferrocene[22] was also unsuccessful, giving rise only to an insoluble black solid. Finally, we discovered that 2-chloro-1,3-dimethylimidazolinium chloride[23] was an effective reagent to convert **13** and **14**, respectively, to **15**[24] and **16** in high yields. However, the purification procedure was relatively tricky. The product needed to be first prepurified by liquid column chromatography on silica gel, using $EtOAc/CH_2Cl_2$ as the eluent. The product collected sometimes contained small amounts of 1,3-dimethylimidazolidin-2-one, the byproduct from the reaction, as the impurity. Fortunately, this polar byproduct could be washed away with MeOH to give essentially pure **15** and **16**.

Amination of **16** under the Buchwald−Hartwig conditions[25] led to **8** in high yield (Scheme 4). On the other hand, Suzuki coupling[26] of **16** with the corresponding boronic acids led to **9**, **10**, and **17** in moderate to high yields.

We have also prepared **21**–**23** from **18** on the basis of similar synthetic strategies that are shown in Scheme 5. Compounds **21**–**23** contained only one triarylamine sidearm and one ferrocene unit. Their electrochemical behaviors were less complicated than those of the target molecules and were used as references in the later voltammetric and spectroelectrochemical studies.

Scheme 5. Synthesis of 21−23

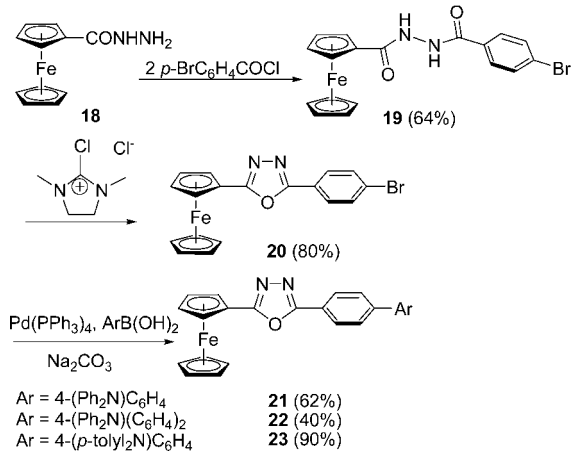

Scheme 6. Synthesis of 11 and 28

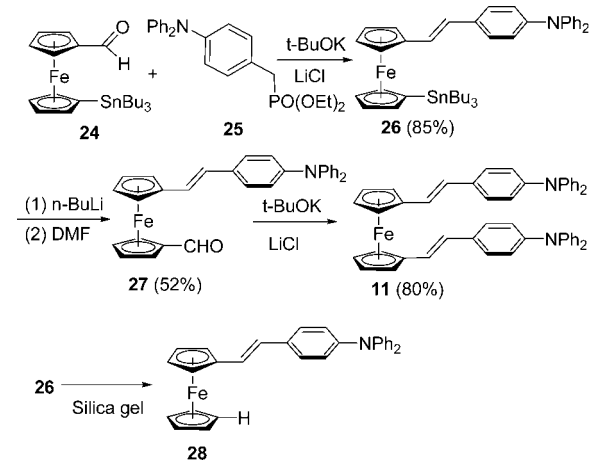

The synthesis of **11** was started from **24**[27] (Scheme 6). The Horner−Wadsworth−Emmons reaction[28] of **24** with **25** under basic conditions provided **26**. Only the trans isomer was isolated from the reaction. The geometry of the olefinic bond was confirmed by the large J^3 coupling constant of 16 Hz. The $(n\text{-}Bu)_3Sn$ substituted compound **26** was then lithiated through a lithium−tin exchange, followed by the reaction with dimethylformamide (DMF) to give the aldehyde **27**. By repeating the Horner−Wadworth−Emmons reaction, **27** was transformed to **11**. It is interesting that **26** was relatively unstable and was partially hydrolyzed on a silica gel during liquid chromatography to give **28**. The trans structure of **28** was further confirmed by X-ray crystallographic analysis.

Single Crystal X-Ray Crystallographic Analyses of 10, 16, and 28. Single crystals of **10**, **16**, and **28** were prepared by the slow evaporation of the solvents. The constitution of **28**, which was obtained by destannylation of

(22) Gonzalez, B.; Alonso, B.; Losada, J.; Garcia-Armada, M. P.; Casado, C. M. *Organometallics* **2006**, *25*, 3558.
(23) Isobe, T.; Ishikawa, T. *J. Org. Chem.* **1999**, *64*, 6984.
(24) Lorkowski, H. J.; Pannier, R.; Wende, A. *J. Prakt. Chem.* **1967**, *35* (3–4), 149.
(25) (a) Hartwig, J. F. *Synlett* **1997**, 2046. (b) Hartwig, J. F. *Angew. Chem., Int. Ed.* **1998**, *37*, 329. (c) Wolfe, J. P.; Wagaw, S.; Marcoux, J.-F.; Buchwald, S. L. *Acc. Chem. Res.* **1998**, *31*, 805. (d) Yang, B. H.; Buchwald, S. L. *J. Organomet. Chem.* **1999**, *576*, 125. (e) Wolfe, J. P.; Wagaw, S.; Buchwald, S. L. *J. Am. Chem. Soc.* **1996**, *118*, 7215. (f) Wolfe, J. P.; Buchwald, S. L. *Tetrahedron Lett.* **1997**, *38*, 6359. (g) Wolfe, J. P.; Buchwald, S. L. *J. Org. Chem.* **2000**, *65*, 1144.
(26) Bellina, F.; Carpita, A.; Rossi, R. *Synthesis* **2004**, *15*, 2419.
(27) (a) Sammakia, T.; Latham, H. A. *J. Org. Chem.* **1996**, *61*, 1629. (b) Roberts, R. M. G.; Silver, J.; Azizian, J. *J. Organomet. Chem.* **1986**, *303*, 387. (c) Wright, M. E. *Organometallics* **1990**, *9*, 853. (d) Nakamura, S.; Fukuzumi, T.; Toru, T. *Chirality* **2003**, *16*, 10. (e) Bolm, C.; Hermanns, N.; Classen, A.; Muniz, K. *Bioorg. Med. Chem. Lett.* **2002**, *12*, 1795.
(28) Motoyoshiya, J. *Trends Org. Chem.* **1998**, *7*, 63.

Table 1. Fe−C Bond Lengths of the Ferrocene Moieties of 10, 16, and 28

	compound **10** (Å)		compound **16** (Å)		compound **28** (Å)	
Cp-ring(1)	Fe–C1	2.047 (4)	Fe–C9	2.041	Fe–C1	2.038
	Fe–C2	2.037 (4)	Fe–C10	2.022	Fe–C2	2.040
	Fe–C3	2.043 (4)	Fe–C11	2.036	Fe–C3	2.027
	Fe–C4	2.040 (4)	Fe–C12	2.051	Fe–C4	2.020
	Fe–C5	2.038 (3)	Fe–C13	2.056	Fe–C5	2.019
Cp-ring(2)	Fe–C38	2.059 (4)	Fe–C14	2.051	Fe–C6	2.050
	Fe–C39	2.034 (4)	Fe–C15	2.047	Fe–C7	2.044
	Fe–C40	2.025 (5)	Fe–C16	2.041	Fe–C8	2.032
	Fe–C41	2.024 (4)	Fe–C17	2.034	Fe–C9	2.030
	Fe–C42	2.034 (4)	Fe–C18	2.044	Fe–C10	2.059

Table 2. C–C Bond Lengths of the Cp Rings of 10, 16, and 28

	compound **10** (Å)		compound **16** (Å)		compound **28** (Å)	
Cp-ring(1)	C5–C1	1.431 (5)	C13–C9	1.425 (5)	C5–C1	1.357 (7)
	C1–C2	1.406 (5)	C9–C10	1.421 (4)	C1–C2	1.357 (7)
	C2–C3	1.399 (6)	C10–C11	1.431 (5)	C2–C3	1.370 (7)
	C3–C4	1.418 (5)	C11–C12	1.410 (6)	C3–C4	1.415 (8)
	C4–C5	1.418 (5)	C12–C13	1.417 (5)	C4–C5	1.408 (8)
Cp-ring(2)	C42–C38	1.421 (5)	C18–C14	1.423 (4)	C10–C6	1.417 (5)
	C38–C39	1.416 (6)	C14–C15	1.423 (4)	C6–C7	1.420 (5)
	C39–C40	1.404 (6)	C15–C16	1.421 (5)	C7–C8	1.399 (5)
	C40–C41	1.406 (5)	C16–C17	1.427 (5)	C8–C9	1.408 (5)
	C41–C42	1.416 (5)	C17–C18	1.425 (5)	C9–C10	1.432 (5)

26 on silica gel, has been verified by X-ray crystallographic analysis, and the C−C and C−Fe bond lengths of the ferrocene units are summarized in Tables 1 and 2.

The single crystal of **28** was $P\bar{1}$ with $Z - 2$, $R(F_o) = 0.0562$ ($I > 2\sigma(I)$) and $R(F_o) = 0.140$ (all data). The substituent effects were reflected on the C–C bond lengths of the cyclopentadienyl (Cp) ring that were unevenly distributed. The bond lengths of 1.357 Å, 1.357 Å, and 1.370 Å for C1–C2, C1–C5, and C2–C3, respectively, were relatively short in comparison to those of 1.415 Å and 1.408 Å for C3–C4 and C4–C5, respectively. On the other hand, the Fe–C bond distances of 2.019, 2.020, and 2.027 for C3, C4, and C5 were shorter than those of 2.038 and 2.040 for C1 and C2, respectively. These observations suggested that the chemical bonding interactions between the Fe atom and the π-array of C3–C5 were relatively strong and desymmetrized the ferrocene group. The Fe atom was located away from the center of the Cp ring and was placed closer to C3–C5. On the other hand, the carbon–carbon bond of C9–C10 was relatively long. The bond length of 1.432(5) was recorded while the other four C–C bonds were 1.399 Å, 1.408 Å, 1.417 Å, and 1.420 Å, respectively. The average C–C bond length of the two Cp rings was 1.398 ± 0.027 Å.

The structures of the other two oxadiazole substituted ferrocenes were somewhat different from those of **28** (Figure 1). The single crystal of **10** was $P2_1/c$ with $Z = 4$, $R(F_o) = 0.0631$ ($I > 2\sigma(I)$) and $R(F_o) = 0.1344$ (all data). The single crystal of **16** was $P2_1/n$ with $Z = 4$, $R(F_o) = 0.0389$ ($I > 2\sigma(I)$) and $R(F_o) = 0.062$ (all data). In spite of the unevenly distributed Cp C–C bond length of **28**, the Cp C–C bond lengths of **10** and **16** were relatively homogeneous. The average C–C bond lengths for **10** and **16** were 1.414 ± 0.009 Å and 1.422 ± 0.006 Å, respectively. The C–C average bond length was slightly larger than that of ferrocene, in which the C–C bond distance of interest was 1.389 Å.[29]

(29) (a) Hughes, R. P.; Kowalski, A. S.; Lomprey, J. R.; Rheingold, A. L. *Organometallics* **1994**, *13*, 2691. (b) Steudel, R.; Hassenberg, K.; Pickardt, J. *Organometallics* **2002**, *21*, 2604.

Noteworthy are the almost eclipsed conformations of the Cp rings and their nearly coplanar π-orbital alignment with the vinyl group of **28** and with the oxadiazole rings of **10** (Figure 2) and **16** (Figure 3). According to the analysis of **28**, the dihedral angle of 8.4° was measured for C6–C10–C11–C12. On the other hand, the dihedral angles of 11.0° and 18.7° for C13–C9–C8–O1 and C14–C18–C19–O2 of **16** as well as the dihedral angles of 20.6° and 25.8° for C1–C5–C6–O1 and C38–C42–C43–O2 of **10**, respectively, were recorded. The nearly coplanar arrangements would allow a strong π-conjugation between the Cp rings of the ferrocene (Fc) unit and the substituents. The redox behavior of the Fc core would therefore be significantly modulated by the electronic

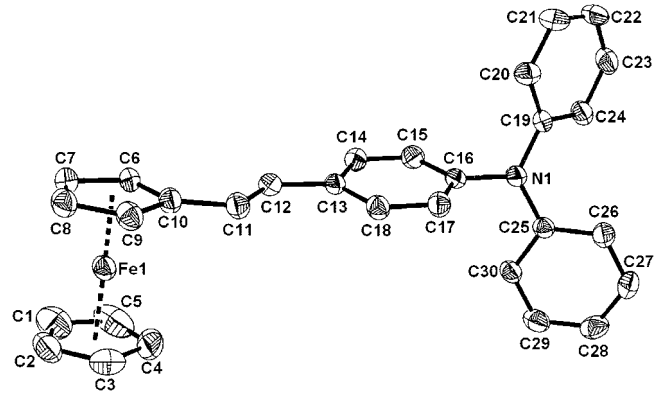

Figure 1. Oak Ridge thermal ellipsoid plot (ORTEP) of **28**.

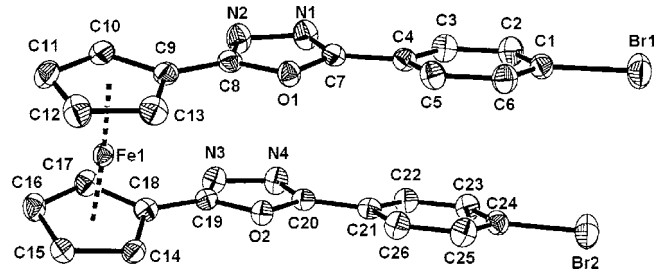

Figure 2. ORTEP of **16**.

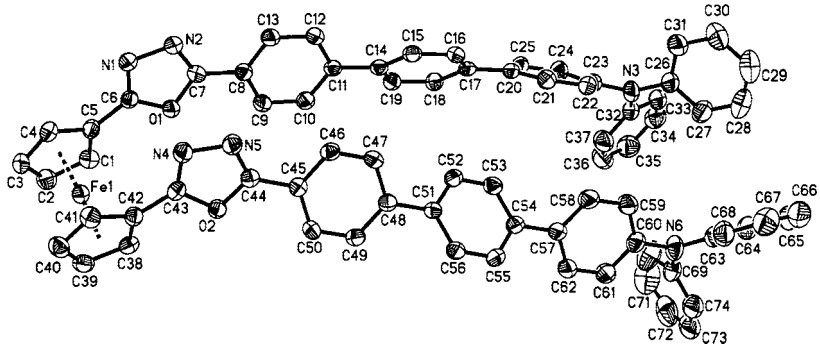

Figure 3. ORTEP of **10**.

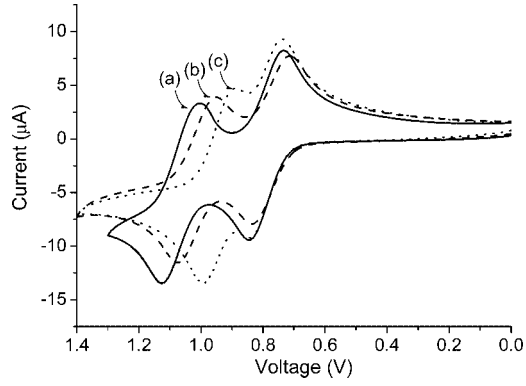

Figure 4. Cyclic voltammetric diagrams of the mono-OXD substituted ferrocenes: (a) **21**, (b) **22**, and (c) **23**.

properties of the organic substituents. This conclusion was in good agreement with the results of later voltammetric studies.

Electrochemical Behavior of the Ferrocene Derivatives. The electrochemical properties of **8**–**11**, **15**, **21**–**23**, and **28** were investigated by cyclic voltammetry (CV) in CH_2Cl_2, using a platinum disk electrode as the working electrode and Bu_4NClO_4 (0.1 M) as the supporting electrolyte. The scan rate was 100 mV/s^{-1}. The applied electrical potential was reported against a AgCl/Ag couple as reference and calibrated in situ against Fc/Fc^+ ($E_{1/2} = 0.51$ V) as an internal standard.

Cyclic Voltammetric Behavior of the Mono-OXD Substituted Ferrocene System. Compounds **21**–**23** showed two oxidation waves in Figure 4; the first one is for the redox couple of Fc/Fc^+ while the second one is for the redox couple of the amino group. These assignments were evidenced on the basis of their spectro-electrochemical behavior that will be discussed in the latter sections.

The half-potential of the Fc/Fc^+ couples fell into a narrow region of 0.80 ± 0.02 V, with the $E_{1/2}^{(1)}$ values showing up at 0.82 V, 0.79 V, and 0.80 V, respectively (Scheme 7). These values were apparently higher in comparsion to that of the ferrocene standard ($E_{1/2}^{Fc/Fc+} = 0.51$ V). We attributed this to the electronic effects arising from the electron-withdrawing properties of the oxadiazole substituents. On the other hand, the electronic effects of the terminal Ph_2N–groups on the Fc/Fc+ couple were small. The variation of the length of the phenylene bridge did not significantly alter the $E_{1/2}^{(1)}$ values of the ferrocene moieties. This result indicated that the blocking effects of the OXD ring are

Scheme 7. Electrochemical Oxidation of 21–23

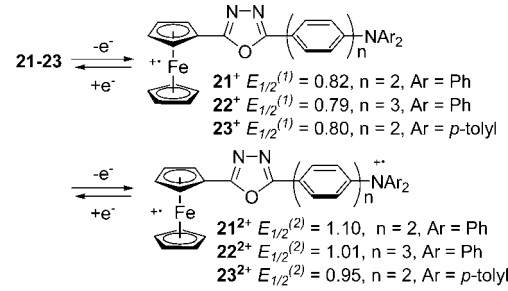

significant. On the other hand, the $E_{1/2}^{(2)}$ values of the second oxidation waves of **21**–**23** covered a relatively wide range. Their $E_{1/2}^{(2)}$ values appeared at 1.10 V, 1.01 V, and 0.95 V, respectively. These values could be explained in terms of a combination of the electronic effects arising from the electron-withdrawing OXD rings as well as the electron-donating methyl substituents. First of all, the presence of the electron-withdrawing OXD rings conjugated to the Ar_2N–groups retarded their electrochemical oxidation. However, when the length of the phenylene bridge increased, the effect of the oxadiazole group on the amino oxidation diminished. Therefore, the lower oxidation potential for the triarylamino moieties of **22** ($E_{1/2}^{(2)} = 1.01$ V) was expected in comparison to that of **21** ($E_{1/2}^{(2)} = 1.10$ V). On the other hand, the presence of electron-donating methyl substituents on the terminal phenyl groups of **23** stabilized the cationic states, leading to a reduction of the oxidation potential to 0.95 V. These results indicated the existence of a strong electronic coupling between the Ar_2N and the OXD groups.

Cyclic Voltammetric Behavior of the Bis-OXD Substituted Ferrocene System. 1,1′-Bis[5-(phenyloxadiazol-2-yl)]ferrocene **15** showed a reversible oxidation wave at $E_{1/2} = 0.95$ V. Because there are two electron-withdrawing oxadiazole rings conjugated with the ferrocene unit, the oxidation of the Fc core of **15** should be relatively difficult in comparison to that of **21**–**23**. This was reflected in the higher Fc/Fc^+ oxidation half-potential of **15** (0.95 V) when comparing against the $E_{1/2}^{(1)}$ of **21**–**23** (0.80 ± 0.02 V).

The oxidation behaviors of **8**–**10**, shown in Figure 5, were similar to those of **21**–**23**. In the first CV cycle of **8** (Figure 5, line d), two anodic waves with peaks at 0.98 V and 1.22 V, respectively, were observed in the forward scan. The maximum current of the first anodic wave was about one-half of that of the second wave, indicating that the second wave corresponded to a two-electron oxidation. Because the

Scheme 8. Electrochemical Oxidation of 8–10

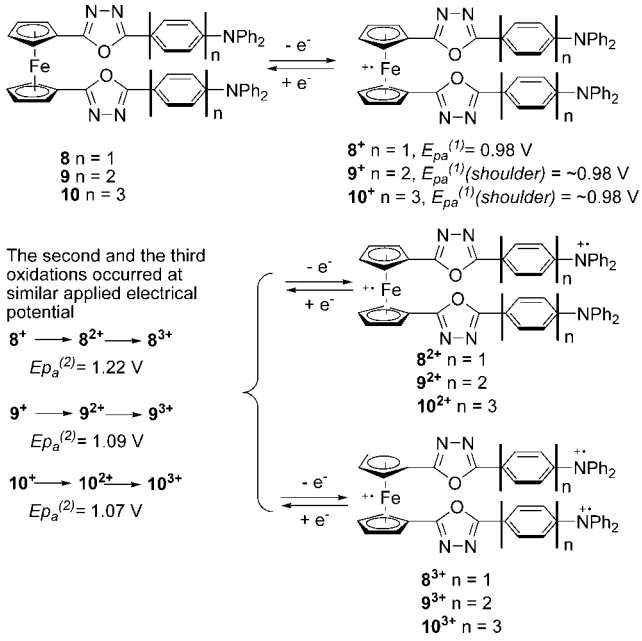

anodic current intensity usually correlated to the number of the oxidation sites on the molecules, we therefore assigned the first wave to the oxidation of the ferrocene unit and the second wave to the oxidation of the triarylamine units (Scheme 8). Because the interactions between two amino groups were blocked by the oxadiazole units, the electronic coupling between the amino lone pairs was expected to be weak. Therefore, the splitting of the $E_{1/2}$ of the second and the third oxidations should be small and could not be resolved. These assignments were further supported by spectro-electrochemical analysis.

Compound **9** showed a major anodic wave, peaking at 1.09 V, with a shoulder that appeared at 0.94 V (Figure 5, line c). The shoulder at 0.94 V was close to the first E_{pa} of **8** at 0.98 V and was assigned to the ferrocene oxidation. Increasing the length of the phenylene ring bridges did not significantly affect the Fc oxidation potential, indicating that the electronic communication between the amino groups and the ferrocene unit was small. On the other hand, the oxidation potential of the triarylamine units of **9** shifted forward to 1.09 V. This could be rationalized because the electron-withdrawing effect arising from the oxadiazole group

Scheme 9. Electrochemical Oxidation of 28

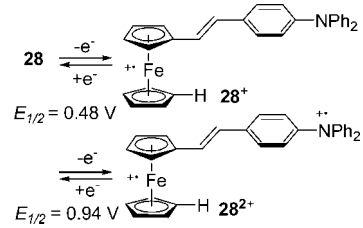

decreased when the length of the phenylene bridge increased. Therefore, the amino units became easily oxidized.

The methyl substituted reference compound **17** showed a broad CV wave, shown as an inset in Figure 12, that ranged from 0.85 to 1.3 V. Although the CV waves covered a similar voltage region as that of **9**, the waves could not be resolved. However, the latter spectro-electrochemical analysis provided the necessary and independent evidence to verify the stepwise oxidation mechanisms.

When the number of the phenylene rings of **10** increased to three, the oxidation waves of the ferrocene unit and the amino cores merged (Figure 5, line b) and became indistinguishable in the cyclic voltammogram.

Cyclic Voltammetric Behavior of the Vinyl Substituted Ferrocene System. When the electron-withdrawing oxadiazole linkers were replaced by vinylene groups, the ferrocene oxidation occurred significantly earlier (Figure 6). The CV of **28** (Scheme 9) showed two waves at $E_{1/2} = 0.48$ and 0.94 V, respectively (Figure 6, line a). The first wave was assigned to the Fc/Fc^+ couple that was further proved in the spectro-electrochemical study. The second wave was due to the redox couple of the amino group. Similar CV features for **11** (Scheme 10) were observed in which the first oxidation occurred slightly earlier at $E_{1/2} = 0.40$ V and the amino oxidations occurred at a similar voltage region, with the E_{pa} at 0.90 and 1.09 V, respectively (Figure 6, line b). The shifts of the $E_{1/2}{}^{Fc/Fc+}$ to the lower voltages of 0.48 V for **28** and 0.40 V for **11** in comparison to the ferrocene standard at 0.51 V were expected in consideration of the π-electron donating ability of the vinyl substituents. Noteworthy is the splitting of the amino oxidation waves in the CV of **11**. Unlike the CV of **8**, the splitting of the amino oxidation waves indicated the existence of a relatively strong electronic coupling between the amino groups through the vinyl–ferrocene–vinyl linker.

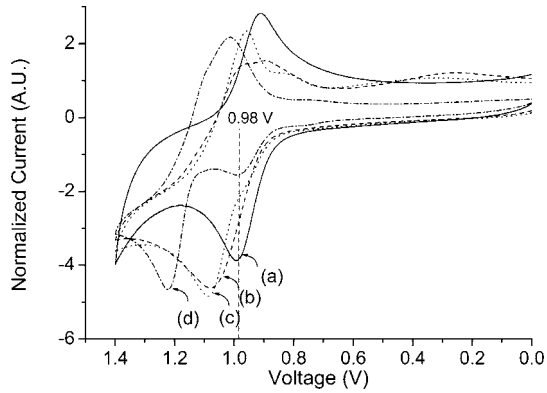

Figure 5. Cyclic voltammetric diagrams of the di-OXD substituted ferrocenes: (a) **15**, (b) **10**, (c) **9**, and (d) **8**.

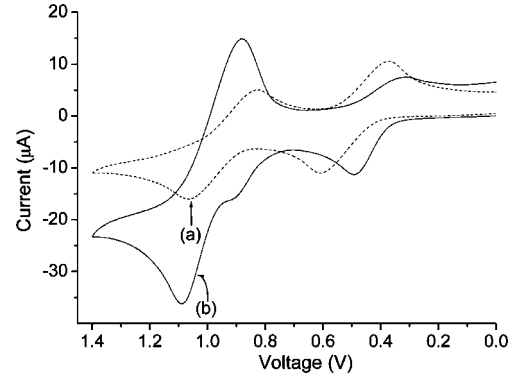

Figure 6. Cyclic voltammetric diagrams of the vinyl substituted ferrocenes: (a) **11** and (b) **28**.

Scheme 10. Electrochemical Oxidation of 11

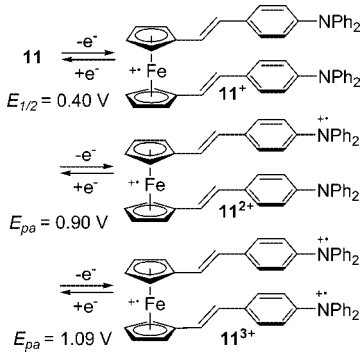

Electropolymerization of 8–11. Upon repetitive scanning for **8–11** over the voltage range from 0 to 1.4 V, new redox patterns were found to grow in intensity on the Pt electrode. An example of **10** is shown in Figure 7. This indicates the formation of the electrochemically active polymeric film of **10** on the electrode surface (Scheme 11). A new wave appeared as a shoulder at 0.85 V since the second scan. As seen in the inset of Figure 7, the absolute value of the anodic current intensity at 0.85 V was linearly proportional to the number of the scan. This is a typical oxidation wave of the benzidine group, indicating the occurrence of the oxidative coupling between $-ArNPh_2$ units.

More important was that similar growth occurred on an indium tin oxide (ITO) glass surface. Because ITO glass is a common transparent conductor, the electropolymerization of the ferrocene—triarylamine containing materials on the electrode surface would modify the electronic properties of the electrode. This surface modification tactic could then be applied to a wide range of optoelectronic device fabrications.

A similar growth of the current intensity was again observed for **11** in the repetitive CV study (Figure 8). Although the splitting of the E_{pa} and E_{pc} of a redox couple, denoted as ΔE_p, usually increased during the electrochemical polymerization, the increment of the potential splitting of the Fc/Fc^+ couple is much larger in comparison to that of the amino units. In the first CV cycle, the ΔE_p values for the Fc/Fc^+ and the $-C_6H_4NPh_2/-C_6H_4NPh_2(+\bullet)$ couples were 0.17 and 0.20 V, respectively. After repeated scanning for 10 cycles, the ΔE_p values for the Fc/Fc^+ and the $-C_6H_4NPh_2/-C_6H_4NPh_2(+\bullet)$ couples increased to 0.55 and 0.42 V, respectively. This result indicated that the oxidation of the ferrocene units was kinetically retarded more seriously than that of the triarylamino moieties during polymerization. This might be due to the fact that steric hindrance around the ferrocene cores was larger, leading to a sluggish diffusion of the counterions when the film thickness increased.

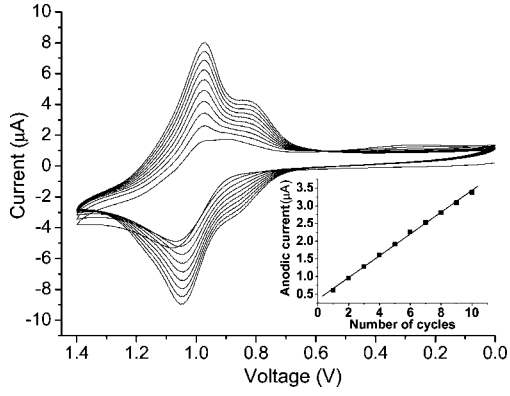

Figure 7. Electropolymerization of **10** on the Pt working-electrode surface. The repetitive scans were performed between 0 and 1.4 V. A pattern change with increasing current intensity was observed. The inset is a linear plot of the absolute value of the anodic current intensity grown at 0.85 V vs the number of scans.

On the contrary, the electropolymerization became ineffective for **17** when the 4-position of the terminal phenyl groups was blocked by the methyl substituents. This result evidenced that the oxidative polymerization of **8–11** occurred at the para-position of the terminal phenyl units.[30]

The CV behavior of the singly Ph_2N- substituted **21** and **22** was quite different from that of **8–10**. Compounds **21** and **22** showed reversible CV patterns (Figure 5) in the electrochemical studies. No current growth or pattern change was observed upon repetitive CV scanning, indicating that the deposition of **21** and **22** was slugguish.

Repetitive scanning for **28** showed a new shoulder wave that appeared at $E_{pa} = 1.05$ V (Figure 9). However, the growth rate of the current intensity was slow, implying that the deposition rate of the electroactive materials on the electrode surface was also sluggish. All this suggested the necessity of having dual diphenylamino side-arms for successful electrochemical depositions.

Spectro-Electrochemical Studies of the Electroactive Species: 9, 11, 15, 17, 21–23, and 28. The spectro-electrochemical experiment[31] is a convenient and effective tool for the elucidation of the reaction mechanisms. A setup of 1 mm thick quartz cuvette equipped with a Pt gauze as the working electrode, a Pt wire as the counter electrode, and a Ag/AgCl electrode as reference were employed. The UV—vis—near-infrared (NIR) absorption spectra of the newly generated electro-active species were directly recorded during electrochemical oxidation. It took about 5 min to reach equilibrium after each voltage adjustment. Through monitoring the change of their absorption spectra, one can collect information about the reaction intermediates in the oxidation processes.

In the following study, we first examined the spectral change of **15** (Figure 10) during the electrochemical oxidation. Because **15** does not contain any amino moiety, we could single out the spectral change of the ferrocene moiety on the basis of the results.

The reference compound **15** started to be oxidized at 0.9 V. When the applied potential was gradually raised from 0.9 to 1.34 V, the ferrocene absorption intensity at 350 nm slightly dropped and a new shoulder band appeared at 400–500 nm with tailing extended to over 700 nm.

Next, the reference compounds **23** and **17** were examined, in which the coupling process was blocked by the introduction of the methyl protective substituents. Because the oxidative coupling process was retarded, the spectral changes were clearly due to the formation of the cationic states of **23** and **17**.

(30) Nelson, R. F.; Adams, R. N. *J. Am. Chem. Soc.* **1966**, *88*, 3498.
(31) Bard, A. J.; Faulkner, L. R. *Electrochemical Methods: Fundamentals and Applications*; Wiley: New York, 2001.

Scheme 11. Electropolymerization of 8–10 through Benzidine Formation

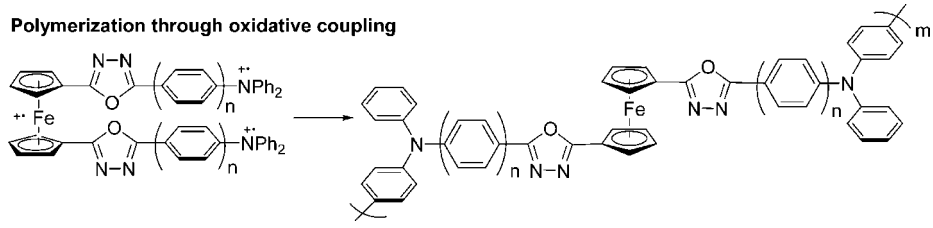

The oxidation of **23** started to occur at 0.66 V (Figure 11). When the applied electrical potential was gradually increased from 0.66 to 0.86 V, the ferrocene absorption band shown at 375 nm decreased and a new absorption shoulder band appeared at 400–500 nm. When the E_{appl} was adjusted to 0.88 V or above, another absorption band originated from the $ArN(tolyl)_2(+\bullet)$ moieties showed up at 600–800 nm.[32,33] These results indicated the occurrence of a two-step oxidation sequence during the oxidation of **23**.

A similar spectral change was observed for compound **17** at the early stage of the oxidation (Figure 12). Although the oxidation waves could not be well-resolved in the CV analysis, the stepwise oxidation processes were clearly evidenced by the spectro-electrochemical experiments. The absorption band between 600 and 800 nm started to appear when the applied potential was set at 0.88 V and reached the maximum at $E_{appl} = 1.0$ V. Parallel to the rising of this band, the ferrocene absorption at 300 nm also dropped. This result illustrated that the first two oxidations occurred almost simultaneously, one for the Fc/Fc^+ couple and the other for the $—ArN(tolyl)_2/-ArN(tolyl)_2(+\bullet)$ couple. The third oxidation appeared later at a higher voltage. Further increase of the applied electrical potential over 1.0 V led to the drop of the absorption intensity at 600–800 nm. This result indicated the occurrence of the third oxidation.

To elucidate the mechanism of the electrochemical coupling reaction, we adopted **21** as an example to study. Because the terminal Ph_2N- group was unprotected in this case, compound **21** would undergo oxidative coupling during the electrochemical study. We have mentioned previously that **21** gave rise to a reversible pattern in the CV scan. Therefore, one may not be able to conclude the occurrence of the oxidative coupling process based on the CV experiment. However, the spectro-electrochemical study provided us an opportunity to re-examine this puzzle. If the oxidative coupling process did occur, the newly formed cationic

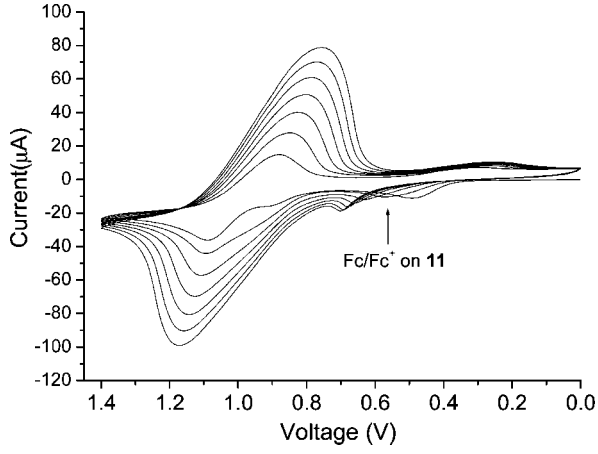

Figure 8. Electropolymerization of **11** on the Pt working-electrode surface. The repetitive scans were performed between 0 and 1.4 V. A pattern change with increasing current intensity was observed.

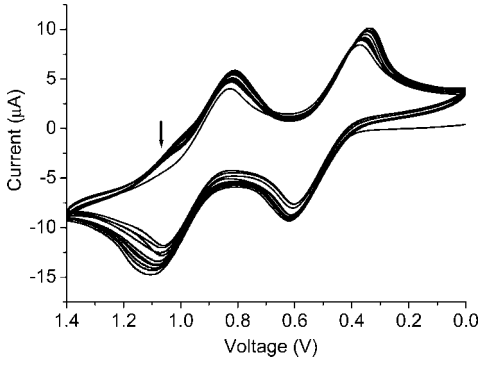

Figure 9. Repetitive CV scans of **28** for 10 cycles. A new shoulder wave, pointed to by an arrow, was observed at $E_{pa} = 1.05$ V.

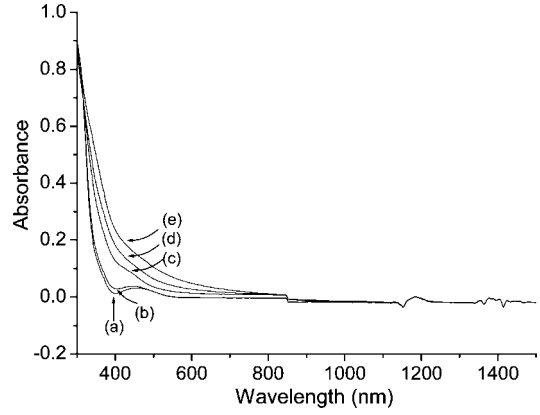

Figure 10. Spectral change of **15** along with increasing of the applied voltage: (a) 0 V, (b) 0.9 V, (c) 1.0 V, (d) 1.1 V, and (e) 1.34 V vs Ag/AgCl couple as reference.

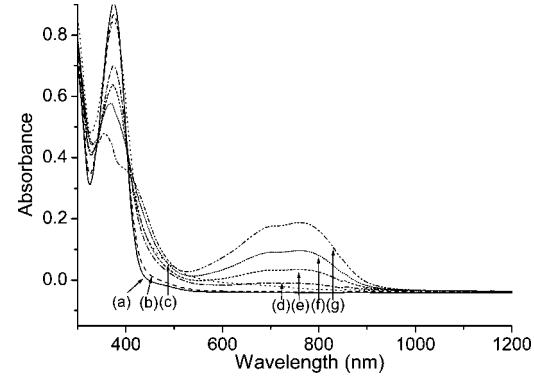

Figure 11. Spectral change of **23** along with increasing of the applied voltage: (a) 0 V, (b) 0.74 V, (c) 0.82 V, (d) 0.90 V, (e) 0.94 V, (f) 0.98 V, and (g) 1.20 V versus Ag/AgCl couple as reference.

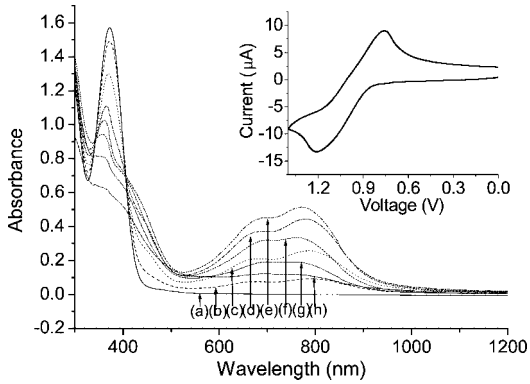

Figure 12. Spectral change of **17** along with increasing of the applied voltage: (a) 0 V; (b) 0.88 V; (c) 0.92 V; (d) 0.96; (e) 1.00 V; (f) 1.06 V; (g) 1.10 V; (h) 1.16 V vs Ag/AgCl couple as reference. Inset is the CV diagram of **17**.

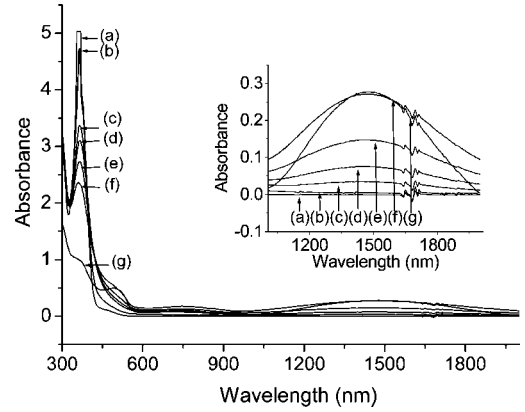

Figure 13. Spectral change of **21** along with increasing of the applied voltage: (a) 0 V, (b) 0.85 V, (c) 0.95 V, (d) 0.97 V, (e) 0.99 V, (f) 1.01 V, and (g) 1.20 V.

benzidine moiety would lead to an intervalence charge-transfer (IVCT) absorption at the NIR region, usually ranged between 1000 and 2000 nm.[18] The results of the spectro-electrochemical experiments could therefore give us a conclusive picture about the oxidative coupling reaction.

Compound **21** was first oxidized at 0.6 V, leading to a drop of the ferrocene absorption intensity at 390 nm. However, when the E_{appl} was raised to 0.88 V or above, unlike **23** which showed an absorption band at 600–800 nm, a new absorption band peaked at 1450 nm arose instead (Figure 13). This characteristic NIR absorption band was arising from the IVCT absorption of the benzidine units,[6b,30,32,33] a product derived from the intermolecular oxidative coupling of the $-C_6H_4NPh_2(+\bullet)$ groups (Scheme 12).

Similar phenomena were observed in the studies of **28** and **8**–**11**. All these supported the oxidative benzidine formation mechanisms in the electropolymerization process.

Electrochemically Deposited Polymer Films (EDPF) as the HIL for PLED Applications. It has long been known that the properties of the hole-injection and hole-transport layers are critical for the performance of the polymeric light emitting devices (PLEDs). The commercially available

Scheme 12. Dimerization of 21 through Oxidative Coupling

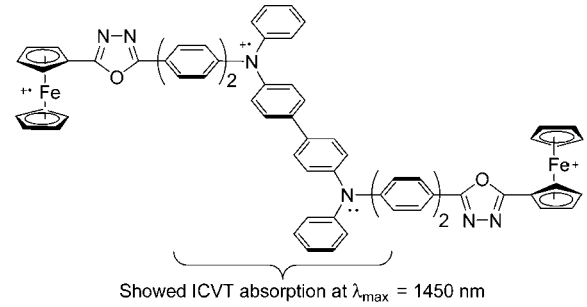

Scheme 13. Electropolymerization of PDPAS

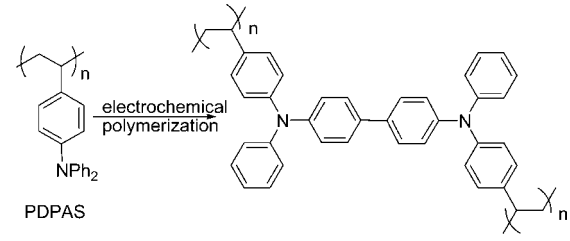

PEDOT-PSS (Bayer Inc.), a conductive polymer system containing poly(3,4-ethylenedioxythiophene) doped with poly(styrenesulfonic acid), has been widely used as the HIL PLED application.[34] Although PEDOT-PSS is a suitable polymeric hole-injection system for most of the applications because of its good electrical conductivity and mechanical strength, the deep green color of the coating might hamper its role on full-color display applications. In our device, we first electrochemically deposited (ED) a layer of **8**, **10**, or **11** directly on ITO by CV. The chemically modified ITO was then washed with CH_2Cl_2 to remove the residual supporting electrolyte. The ITO plate was then dried under vacuum at 100 °C for 30 min, followed by spin-coating (3000 rpm, 90 s) an emissive layer of PVK-Ir(PPy)$_3$-PBD[35] on top. The emissive layer was then dried under vacuum at 100 °C for another 30 min. The composition of the solution used to construct the emissive layer is PVK/Ir(PPy)$_3$/PBD = 100:20:40 mg in $CHCl_3$ (8 mL). The solution was filtered through a PVDF filter (0.2 μm) before use under a clean environment. Finally, a metallic cathode of Mg/Ag was fabricated by thermal evaporation and deposition under vacuum. The overall structure of the devices used in the study is ITO/ED-HIL/PVK:Ir(PPy)$_3$:PBD (50 nm)/Mg (2 nm)/Ag (100 nm). In additon, a device of ITO/PEDOT-PSS (30 nm)/PVK:Ir(PPy)$_3$:PBD (50 nm)/Mg (2 nm)/Ag (100 nm) was used as a standard device for comparison. Since it has been known in literature that poly(4-(*N*,*N*-diphenylaminostyrene) (PDPAS) could be electropolymerized on the electrode surface, we have also adopted this electrochemically deposited thin film as a reference for comparison[36] (Scheme 13).

The layers of **8**, **10**, or **11** were prepared by repetitive scanning over the voltage range from 0 to 1.3 V. The film

(32) Amthor, S.; Noller, B.; Lambert, C. *Chem. Phys.* **2005**, *316*, 141.
(33) Low, P. J.; Paterson, M. A. J.; Goeta, A. E.; Yufit, D. S.; Howard, J. A. K.; Cherryman, J. C.; Tackley, D. R.; Brown, B. *J. Mater. Chem.* **2004**, *14*, 2516.
(34) (a) Cao, Y.; Yu, G.; Zhang, C.; Menon, R.; Heeger, A. J. *Synth. Met.* **1997**, *87*, 171. (b) Berntsen, A.; Croonen, Y.; Liedenbaum, C.; Schoo, H.; Visser, R.-J.; Vleggaar, J.; van de Weijer, P. *Opt. Mater.* **1998**, *9*, 125.
(35) (a) Kohler, A.; Wilson, J. S.; Friend, R. H. *Adv. Mater.* **2002**, *14*, 701. (b) Beeby, A.; Bettington, S.; Samuel, I. D. W.; Wang, Z. *J. Mater. Chem.* **2003**, *13*, 80.
(36) Compton, R. G.; Laing, M. E.; Ledwith, A.; Abu-Abdoun, I. I. *J. Appl. Electrochem.* **1988**, 431.

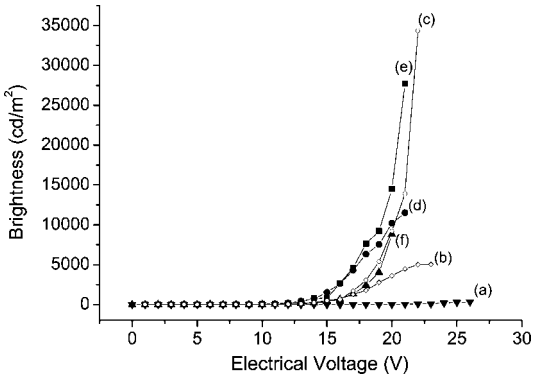

Figure 14. Brightness vs voltage curves for devices 1–6. (a) device 1 (▼); (b) device 2 (◇); (c) device 3 (○); (d) device 4 (●); (e) device 5 (■); (f) device 6 (▲).

Table 3. Comparison of the Device Performances of the PLEDs with Different Types of HIL Layer

device	HIL	maximum efficiency[a]	turn-on voltage[b]	maximum brightness[c]
1	no HIL	1.1	23	320
2	PEDOT-PSS	22.5	12.5	5040
3	ED-HIL of PDPAS	11.5	13	34400
4	ED-HIL of **8**	8.0	11	11500
5	ED-HIL of **10**	11.3	11	27700
6	ED-HIL of **11**	4.3	13	11200

[a] cd/A. [b] V, at 100 cd/m^2. [c] cd/m^2.

was almost colorless to slightly yellowish after deposition, with the CV scans ended at 0 V. The optimized scan number for the PLED was two to three cycles. The brightness versus voltage curves are shown in Figure 14. Their performances are summarized in Table 3.

Without being modified by any HIL, the reference device of ITO/PVK-Ir(PPy)$_3$-PBD/Mg-Ag showed the turn-on voltage of 23 V, with the maximum brightness of 320 cd/m^2 and the current efficiency of 1.10 cd/A. The high turn-on voltage was due to the high energy barrier for the hole-injection process from the ITO electrode into the emissive PVK layer. When the ITO surface was modified by a PEDOT-PSS coating, the hole-injection energy barrier was significantly reduced so that the turn-on voltage dropped significantly to 12.5 V, with the current efficiency going up to 22.5 cd/A. The high current efficiency of the PEDOT-PSS modified PLEDs was probably due to the balanced hole and electron injection processes. However, the brightness versus voltage curve climbed up slowly when the applied electrical potential increased. The maximum brightness could only reach 5040 cd/m^2. On the other hand, when an electrochemically deposited layer of PDPAS (MW: 2800, PDI = 1.45) was used, the turn-on voltage of 13 V was slightly higher than that of the PEDOT-PSS device. However, the maximum brightness could be boosted up to 34 400 cd/m^2 with the maximum current efficiency of 11.5 cd/A.

When **8** was used, the PLED performance was also improved dramatically in comparsion to the primitive device. The turn-on voltage was reduced to 11 V, with the maximum brightness of 11 500 cd/m^2 and the current efficiency of 8.0 cd/A. When **10** was used the turn-on voltage was 11 V, with the maximum brightness of 27 700 cd/m^2 and the current efficiency of 11.3 cd/A. These results indicated that the electrochemically deposited layers were good hole-injecting layers that could significantly reduce the energy barrier of the hole-injection process. It is noteworthy that the turn-on voltage of the devices 4 and 5 were even lower than that of the PEDOT-PSS modified device 2. On the contrary, the PDPAS did not show such a turn-on voltage reduction effect. These results reflected that the ferrocene core played an important role on the reduction of the turn-on voltage of the PLED. Perhaps because of the unbalanced hole injection over electron injection, the device efficiency, on the other hand, decreased.

When **11** was used as the precursor for the hole-transport layers, the turn-on voltage increased to 13 V, with the maximum brightness of 9000 cd/m^2 and the current efficiency of 3.8 cd/A. The turn-on voltage was apparently higher than that of the devices 4 and 5 and close to that of device 3. We are reminded that the $E_{1/2}$ of the Fc core was 0.5 V lower than that of the corresponding benzidine linker in this case. Some Fc^+ cations might therefore be formed as space charges and trapped in the benzidine matrix. The mobility of this type of positive charge might be low and would only have a small contribution to the hole-injection process. However, the presence of excessive positive charges trapped in the matrix might inhibit the hole-injection process, leading to an increment of the hole-injection energy barrier and a consequently increased turn-on voltage. In addition, electrons might migrate into the layer and recombine with the Fc^+. Because this process would only consume the electrical current without a contribution to the light emitting function, the current efficiency of the PLEDs would therefore be reduced, leading to a low current efficiency of 4.3 cd/A.

Scanning Electron Microscopy (SEM) Studies of the Polymeric Films of 8, 10, and 11 on ITO Glass. The high performance of the devices attracted us to further investigate the morphology of the electrochemically deposited thin films on ITO. The thickness of the films was evaluated by an alpha-step instrument. The morphology of the films was studied by using field-emission SEM (15 KV) with magnification of 1.2×10^5 times. The films were prepared under the same conditions as those for PLED fabrication.

The thickness of the electrochemically deposited layers from the CV method was indeed very thin. The film thicknesses were estimated to be less than 10 nm according to the alpha-step measurement. Figure 15 shows SEM images obtained from the bare ITO glass, purchased from the Merck company, and the thin films of **8**, **10**, and **11** on the ITO plates for comparison. The granular structure of the bare ITO glass was observed (Figure 15a), with the diameters around 10–20 nm, in the SEM study. When the ITO was treated with electropolymerization, the polymeric materials were evenly deposited onto the surface (Figure 15b−d). Because the thickness of the layers was thin, the presence of the deposition layers only slightly altered the morphology of the ITO surface and the granular patterns could still be observed. However, the presence of the thin layers significantly altered the properties of the electrode, leading to a reduction of the turn-on voltage of the PLEDs.

In summary, we demonstrated the use of diphenylamino substituted ferrocenes as effective precursors for electro-

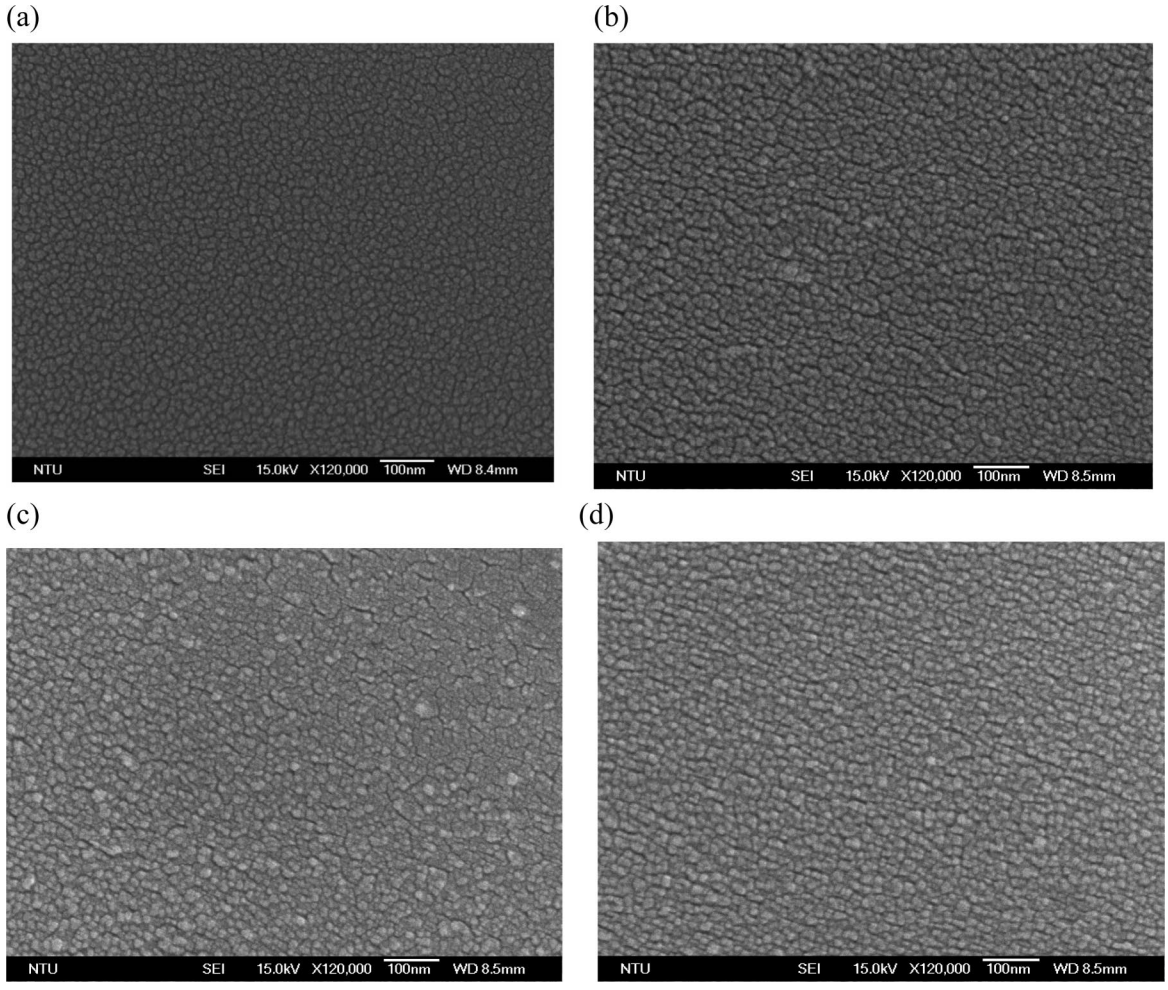

Figure 15. Field-emission SEM images (15 KV) of the (a) bare ITO and the electrochemically deposited polymeric films of (b) **8**, (c) **10**, and (d) **11** on ITO glass. The films were prepared by repetitive CV scan of the precursor solutions for three cycles. The images were enlarged 120 000 times. The samples were treated with sputttering of Pt onto the surface before the SEM image collection.

chemical deposition. The deposition tactics were successful, providing a new route to access ferrocene-based organic−organometallic hybrid polymeric thin films. The hole-injection performance of the films on PLED applications was indeed outstanding and led to low turn-on voltage of the PLEDs. Although the detailed mechanisms in the present cases were uncertain, previous research reports revealed that ferrocene containing redox-active polymeric materials that possessed controllable, spacer mediated metal−metal interactions would have interesting hole-transport properties.[37] In particular, the electrical conductivity of those materials would be largely increased by 10 orders of magnitude after partial oxidation and up to semiconductor values. Perhaps similar mechanisms operated in the present cases. The ferrocene containing layer that was coated onto the ITO surface would be partially oxidized when the electrical potential was applied. The hole-transport properties and conductivity would therefore be enhanced. This would be beneficial for the hole-injection and transport processes to take place, lowering the turn-on voltage of the PLEDs.

Experimental Section

Hexane and ethylacetate were dried over anhydrous $CaCl_2$. Dichloromethane was dried over P_2O_5 or CaH_2. Diethylether and tetrahydrofuran (THF) was dried over Na metal plates, using benzophenone as an indicator. All the solvents were freshly distilled before use.

***N,N′*-Bis(4-bromobenzoyl)-1,1′-ferrocenedicarbohydrazide (14).** To a solution of 1,1′-ferrocenedicarbohydrazide (4.1 g, 15 mmol) in *N*-methylpyrrolidone (NMP, 15 mL) at 0 °C was added 4-bromobenzoyl chloride (6.72 g, 30 mmol) under nitrogen. After reaction for 1 h, the reaction mixture was gradually poured into ice–water (500 mL). The product precipitated from the aqueous solution. The yellowish precipitates were collected by suction filtration and dried to give a yellowish powder **14** (9.34 g, 83%). ^{1}H NMR (400 MHz, DMSO-d_6): δ 10.56 (s, 2H, N−H), 9.93 (s, 2H, N−H), 7.81 (d, J = 8.0 Hz, 4H, Ar−H), 7.71 (d, J = 8.0 Hz, 4H, Ar−H), 4.94 (m, 4H, Cp−H), 4.61 (m, 4H, Cp−H). ^{13}C NMR (100 MHz, DMSO-d_6): δ 168.9, 166.0, 131.9, 131.4, 129.7, 126.1, 74.8, 73.1, 70.4. HRMS-FAB *m/z*: calcd for $C_{26}H_{20}O_4N_4Br_2Fe$, 665.9201; found, 665.9208.

(37) (a) Massey, J. A.; Power, K. N.; Winnik, M. A.; Manner, I. *Adv. Mater.* **1998**, *10*, 1559. (b) Rulkens, R.; Perry, R.; Lough, A. J.; Manners, I.; Lovelace, S. R.; Grant, C.; Geiger, W. E. *J. Am. Chem. Soc.* **1996**, *118*, 12683. (c) Rulkens, R.; Gates, D. P.; Pudelski, J. K.; Balaishis, D.; McIntosh, D. F.; Lough, A. J.; Manner, I. *J. Am. Chem. Soc.* **1997**, *119*, 10976. (d) Rulkens, R.; Resendes, R.; Verma, A.; Manners, I.; Murti, K.; Fossum, E.; Miller, P.; Matyjaszewski, K. *Macromolecules* **1997**, *30*, 8165.

Bis-1,1′-(5-(4-bromophenyl)-1,3,4-oxadiazol-2-yl)ferrocene (16). To a solution of **14** (6.68 g, 10 mmol) and DMC (4.2 g, 25 mmol) in dichloromethane (30 mL) at 0 °C under N_2 was added Et_3N (5.30 mL, 40 mmol). The mixture was stirred for 1 h in an ice bath and warmed gradually to room temperature. After the reaction was complete, the reaction was quenched by addition of water. The product was extracted with CH_2Cl_2 (100 mL × 2). The combined extracts were dried (anhydrous $MgSO_4$), filtered, and concentrated by rotary evaporation. The collected crude solid residue was purified by using liquid chromatography on silica gel, using EtOAC/CH_2Cl_2 = 1:1 as eluent to give an orange solid **16** (5.80 g, 92%): mp 240–241 °C. ^{1}H NMR (400 MHz, $CDCl_3$): δ 7.65–7.62 (m, 4H, Ar−H), 7.52–7.49 (m, 4H, Ar−H), 5.07 (m, 4H, Cp−H), 4.55 (m, 4H, Cp−H). ^{13}C NMR (100 MHz, $CDCl_3$): δ 164.9, 163.0, 132.0, 127.8, 126.0, 122.3, 72.2, 69.7, 68.6. HRMS-FAB *m*/*z*: calcd for $C_{26}H_{17}O_2N_4Br_2Fe(^{79}Br,^{81}Br)$, 632.9047; found, 632.9041.

1,1′-Bis(5-(4-(*N*,*N*-diphenylamino)phenyl)-1,3,4-oxadiazol-2-yl)ferrocene (8). To a mixture of **16** (0.19 g, 0.3 mmol), $Pd(OAc)_2$ (2.5 mg, 0.0089 mmol), DPPF (7.70 mg, 0.01 mmol), and NaO′Bu (0.23 g, 2.23 mmol) in toluene (5 mL) was added diphenylamine (0.11 g, 0.6 mmol) under N_2. The mixture was heated at reflux for 12 h. When the reaction was complete, the reaction was quenched by addition of water. The crude product was extracted twice with CH_2Cl_2. The combined extracts were washed with water, dried (anhydrous $MgSO_4$), filtered, and concentrated by rotary evaporation. The concentrated crude product was purified by liquid chromatography on silica gel, using a mixture of EtOAc and $CHCl_3$ (1/6) as eluent to give a red-brownish solid **8** (0.13 g, 82%): mp 120–121 °C. ^{1}H NMR (400 MHZ, $CDCl_3$): δ 7.73 (d, J = 8.8 Hz, 4H, Ar−H), 7.28–7.23 (m, 8H, Ar−H), 7.13–7.07 (m, 12H, Ar−H), 7.01 (d, J = 8.8 Hz, 4H), 5.02 (m, 4H, Cp−H), 4.47 (m, 4H, Cp−H). ^{13}C NMR (100 MHz, $CDCl_3$): δ 164.1, 163.8, 150.4, 146.5, 129.4, 127.7, 125.4, 124.1, 121.0, 115.9, 72.2, 69.4, 69.0. HRMS-FAB *m*/*z*: calcd for $C_{50}H_{36}O_2N_6Fe$, 808.2249; found, 808.2258. Anal. Calcd for $C_{50}H_{36}O_2N_6Fe$: C, 74.26; N, 10.39; H, 4.48. Found: C, 74.57; N, 10.09; H, 4.08.

Suzuki coupling of **16** and **20** with arylboronic acids was used as a general procedure for the preparation of **9**–**10**, **17**, and **21**–**23**.

1,1′-Bis(5-(4′-(*N*,*N*-diphenylamino)bipheny-4-yl)-1,3,4-oxadiazol-2-yl)ferrocene (9). A mixture of **16** (1.90 g, 3 mmol), 4-(*N*,*N*′-diphenylamino)phenylboronic acid (2.9 g, 10 mmol), $Pd(PPh_3)_4$ (0.4 g, 0.3 mmol), and Na_2CO_3 (1.3 g, 12.0 mmol) in toluene (30 mL) and water (10 mL) under nitrogen was heated at 105 °C for 8 h. When the reaction was complete, water was added and the organic layer was extracted with $CHCl_3$ (150 mL ×2). The extracts were combined and washed twice with water, dried (anhydrous $MgSO_4$), filtered, and concentrated by rotary evaporation. The crude solid obtained was purified by liquid column chromatography on silica gel, using EtOAc−$CHCl_3$ as eluent (1/6) to give a red-brown solid **9** (1.80 g, 62%): mp 296–297 °C. ^{1}H NMR (400 MHZ, $CDCl_3$): δ 7.86–7.84 (d, J = 7.8 Hz, 4H, Ar−H), 7.52–7.50 (d, J = 7.8 Hz, 4H, Ar−H), 7.42–7.40 (d, J = 8.8 Hz, 4H, Ar−H), 7.27–7.23 (m, 8H, Ar−H), 7.12–7.01 (m, 16H, Ar−H), 5.09 (m, 4H, Cp−H), 4.55 (m, 4H, Cp−H). ^{13}C NMR (100 MHz, $CDCl_3$): δ 164.7, 163.8, 147.8, 147.2, 143.2, 133.0, 129.2, 127.6, 127.0, 126.5, 124.6, 123.2, 121.6, 72.2, 69.7, 68.8. HRMS-FAB *m*/*z*: calcd for $C_{62}H_{44}O_2N_6Fe$, 960.2875; found, 960.2892. Anal. Calcd for $C_{62}H_{44}O_2N_6Fe$: C, 77.50; N, 8.75; H, 4.62. Found: C, 77.91; N, 8.86; H, 4.29.

1,1′-Bis(5-(4″-(*N*,*N*-diphenylamino)-1,1′:4′,1″-terphenyl-4-yl)-1,3,4-oxadiazol-2-yl)ferrocene (10). Compound **16** (0.22 g, 0.3 mmol), $Pd(PPh_3)_4$ (0.06 g, 0.05 mmol), 4′-(*N*,*N*′-diphenylamino-)biphenyl-4-ylboronic acid (0.55 g, 1.5 mmol), and Na_2CO_3 (0.21 g, 2.0 mmol) in toluene (7 mL) and water (2 mL) were reacted to give a red-brownish solid **10** (0.15 g, 40%): mp 244–245 °C. ^{1}H NMR (400 MHZ, $CDCl_3$): δ 7.88 (d, J = 8.4 Hz, 4H, Ar−H), 7.59–7.48 (m, 12H, Ar−H), 7.47 (d, J = 8.4 Hz, 4H, Ar−H), 7.26–7.22 (m, 8 H, Ar−H), 7.11–7.10 (m, 12H, Ar−H), 7.03–7.00 (m, 4H, Ar−H), 5.10 (m, 4H, Cp−H), 4.57 (m, 4H, Cp−H). ^{13}C NMR (100 MHz, $CDCl_3$): δ 164.8, 163.7, 147.4, 147.3, 143.2, 140.1, 137.8, 133.8, 129.2, 127.5, 127.2, 126.94, 126.91, 126.90, 124.4, 123.5, 123.0, 122.2, 72.1, 69.8, 69.0. HRMS-FAB *m*/*z*: calcd for $C_{74}H_{52}O_2N_6Fe$, 1112.3501; found, 1112.3514. Anal. Calcd for $C_{74}H_{52}O_2N_6Fe$: C, 79.85; N, 7.55; H, 4.71. Found: C, 79.91; N, 7.17, H, 4.33.

1-(Tri-*n*-butylstannyl)-1′-(4-(*N*,*N*-diphenylamino)styryl)ferrocene (26). To a solution of **24** (5.7 g, 11.4 mmol), diethyl 4-(*N*,*N*-diphenylamino)benzylphosphonate (**25**, 4.5 g, 11.4 mmol), and LiCl (0.95 g, 22.5 mmol) in DMF (50 mL) under nitrogen at 0 °C was added *t*-BuOK (5.6 g, 50 mmol). The mixture was further reacted at 0 °C for 2 h and gradually warmed to room temperature. The reaction was monitored by thin-layer chromatography. When the reaction was complete, water was added to quench the reaction. The crude mixture was extracted twice with Et_2O. The combined extracts were washed with water, dried (anhydrous $MgSO_4$), filtered, and concentrated by rotary evaporation. The crude mixture was purified by column chromatography on silica gel, using hexane−CH_2Cl_2 (4/1) as eluent to afford **25** as a red oil (7.3 g, 86%). ^{1}H NMR (400 MHz, $CDCl_3$): δ 7.3–7.21 (m, 6H, Ar−H), 7.10–7.07 (m, 4H Ar−H), 7.02–6.97 (m, 4H, Ar−H), 6.73 (d, J = 16 Hz, 1H, vinyl−H), 6.61 (d, J = 16 Hz, 1H, vinyl−H), 4.37 (m, 2H, Cp−H), 4.30 (m, 2H, Cp−H), 4.19 (m, 2H, Cp−H), 3.94 (m, 2H, Cp−H), 1.59–1.50 (m, 6H), 1.38–1.25 (m, 6H), 1.03–1.01 (m, 6H), 0.99–0.86 (m, 9H). ^{13}C NMR (100 MHz, $CDCl_3$): δ 147.1, 146.0, 132.0, 128.8, 126.2, 125.2, 125.0, 123.84, 123.76, 122.4, 83.5, 75.6, 72.0, 69.2, 69.0, 66.7, 29.6, 27.8, 14.2, 10.8. HRMS-FAB *m*/*z:* calcd for $C_{42}H_{51}NSnFe$, 745.2393; found, 745.2401.

NMR data of **28** obtained from hydro-destannylation on silica gel are as follows. ^{1}H NMR (400 MHz, $CDCl_3$): δ 7.33–7.12 (m, 6H, Ar−H), 7.12–7.10 (m, 4H Ar−H), 7.05–7.00 (m, 4H, Ar−H), 6.76 (d, J = 16 Hz, 1H, vinyl−H), 6.65 (d, J = 16 Hz, 1H, vinyl−H), 4.45 (m, 2H, Cp−H), 4.27 (m, 2H, Cp−H), 4.15 (s, 5H, Cp−H). ^{13}C NMR (100 MHz, $CDCl_3$): δ 147.6, 146.5, 132.4, 129.3, 126.7, 125.7, 125.4, 124.3, 124.2, 122.9, 84.2, 69.7, 69.4, 67.2. The X-ray data was discussed in the article.

1′-(4-(*N*,*N*-Diphenylamino)styryl)ferrocenecarboxaldehyde (27). The synthesis of **27** was performed according to the procedure for **24**. Compound **26** (1.64 g, 2.2 mmol) in THF (10 mL) under N_2 at −78 °C was reacted first with *n*-BuLi in *n*-hexane (1.6 M, 2 mL, 3.2 mmol), followed by DMF (0.25 mL, 3.0 mmol) to give a crude oil that was purified by column chromatography on silica gel, using EtOAc to give **27** (0.47 g, 52%). ^{1}H NMR (400 MHZ, $CDCl_3$): δ 9.91 (s, 1H, CHO), 7.32–7.24 (m, 6H, Ar−H), 7.12–7.10 (m, 4H, Ar−H), 7.04–7.01 (m, 4H, Ar−H), 6.69 (d, J = 16 Hz, 1H, vinyl−H), 6.25 (d, J = 16 Hz, 1H, vinyl−H), 4.75 (m, 2H, Cp−H), 4.56 (m, 2H, Cp−H), 4.54 (m, 2H, Cp−H), 4.36 (m, 2H, Cp−H). ^{13}C NMR (100 MHz, $CDCl_3$): δ 192.9, 147.0, 146.6, 131.1, 128.9, 127.3, 126.5, 124.0, 123.3, 122.64, 122.60, 85.9, 79.7, 74.4, 70.6, 70.3, 68.0. HRMS-FAB *m*/*z*: calcd for $C_{31}H_{25}NOFe$, 483.1286; found, 483.1291.

1,1′-Bis(4-(*N*,*N*-diphenylamino)styryl)ferrocene (11). Compound **11** was synthesized according to the general synthetic procedure for **26**. Compound **27** (0.45 g, 1.14 mmol), diethyl 4-(*N*,*N*′-diphenylamino)benzylphosphonate (**25**, 0.47 g, 1.2 mmol), and LiCl (0.1 g, 2.4 mmol) in DMF(10 mL) were reacted with *t*-BuOK (0.67 g, 6 mmol) to afford a crude oil that was purified by column chromatography on silica gel, using a mixture of CH_2Cl_2 and hexanes (1/6) as eluent to provide **11** as a red oil (0.7 g, 85%):

mp 210–211 °C. ^{1}H NMR (400 MHZ, $CDCl_3$): δ 7.26–7.21 (m, 12H, Ar−H), 7.11–7.08 (m, 8H, Ar−H), 7.02–6.98 (m, 8H, Ar−H), 6.72 (d, J = 16 Hz, 2H, Ar−H), 6.63 (d, J = 16 Hz, 2H, Ar−H), 4.40 (m, 4H, Cp−H), 4.26 (m, 4H, Cp−H). ^{13}C NMR (100 MHz, $CDCl_3$): δ 147.0, 145.9, 131.8, 128.7, 126.2, 125.5, 124.2, 123.8, 123.5, 122.4, 84.4, 70.0, 68.0. HRMS-FAB *m/z:* calcd for $C_{50}H_{40}N_2Fe$, 724.2541; found, 724.2555. Anal. Calcd for $C_{50}H_{40}N_2Fe$: C, 82.87; N, 3.87; H, 5.56. Found: C, 82.68; N, 4.00; H, 5.02.

Acknowledgment. The present research project was supported by the National Science Council, Taiwan (NSC 95-2113-M-002-020).

Supporting Information Available: The synthetic procedures for **13**, **15**, **17**, and **20**–**24**, ^{1}H and ^{13}C NMR of **8**–**17** and **20**–**28** (PDF), and CIF files for **10**, **16**, and **28**. This material is available free of charge via the Internet at http://pubs.acs.org.

CM702217U